Limnol. Oceanogr., 57(5), 2012, 1555–1571

doi:10.4319/lo.2012.57.5.1555

Nitrate–nitrite dynamics and phytoplankton growth: Formulation and experimental evaluation of a dynamic model

Martino E. Malerba,[a,b,c,*] Sean R. Connolly,[c,d] and Kirsten Heimann [c,e]

[a] AIMS@JCU, James Cook University, Townsville, Queensland, Australia
[b] Australian Institute of Marine Science, Townsville, Queensland, Australia
[c] School of Marine and Tropical Biology, James Cook University, Townsville, Queensland, Australia
[d] Australian Research Council Centre of Excellence for Coral Reef Studies, James Cook University, Townsville, Queensland, Australia
[e] Centre for Sustainable Tropical Fisheries and Aquaculture, Townsville, Queensland, Australia

Abstract

A multi-nutrient quota model was modified to describe the coupled dynamics of nitrate and nitrite utilization for four phytoplankton species, *Picochlorum atomus* (Butcher) (Chlorophyta), *Nannochloropsis oculata* (Droop) (Ochrophyta), *Isochrysis* sp. (Haptophyta), and *Pyrocystis lunula* (Schütt) (Dinophyta). Although rarely considered in nutrient-limited phytoplankton models, nitrite can be an important nitrogen source, as it can be either released due to incomplete reduction of nitrate or taken up to supplement low nitrogen availability. The model accurately characterizes the dynamics of nitrite uptake and excretion, nitrate uptake and assimilation efficiency, and population growth for the study species in batch culture, despite the fact that the species display a range of qualitatively different nutrient utilization patterns. The good performance of the model suggests that per-capita secretion and re-assimilation of nitrite, together with changes to the per-capita internal nitrogen supply, can be inferred from daily observations of medium nitrate and nitrite utilization and population growth. The model also reproduces qualitative characteristics of nitrite dynamics that have been observed in previous empirical studies, such as a rise in per-capita nitrite secretion when culture medium nitrate concentrations and intracellular nitrogen levels are high. Our model therefore provides a new framework for evaluating the potential broader trophic consequences of the effects of nitrite uptake and release on the dynamics of phytoplankton populations.

For the past five decades, there has been extensive research on understanding dissolved inorganic nitrogen levels in the oceans and how they drive primary production of phytoplankton communities (Dugdale 1967; Platt et al. 1989). Among the main forms of dissolved inorganic nitrogen (i.e., ammonia, nitrate, and nitrite), phytoplankton nitrite uptake has been the least investigated (Sciandra and Amara 1994). Many phytoplankton species have been observed to take up and release significant amounts of nitrite (Collos 1982*a*,*b*; Fierro et al. 2008), but both the dynamics and overall extent of this process are still mainly unknown (Sciandra and Amara 1994). Failing to adequately account for the dynamics of nitrite uptake and release may bias predictions of total assimilated nitrogen and primary production of phytoplankton communities (Collos 1998). This is especially the case near the nitricline at the bottom of the euphotic zone, where high nitrite concentrations are commonly encountered (Al-Qutob et al. 2002). Nitrite dynamics are also important in aquaculture, because optimal nitrogen supply should be calibrated to achieve high phytoplankton productivity while avoiding costly wastewater treatments associated with excess nitrogen concentration (Lardon et al. 2009; Yang et al. 2011). More recent research focuses on the potential use of phytoplankton for the remediation of carbon dioxide and nitric oxide from industrial flue gas. A detailed knowledge of nitrite dynamics by different phytoplankton groups is required because nitric oxide is converted 1 : 1 to nitrite in water (Zheng et al. 2011). Thus, an oversupply of nitrate to flue gas–fed phytoplankton cultures can negatively affect nitric oxide remediation and population growth.

Plants convert nitrate to ammonium for incorporation into nitrogen-containing organic molecules using a two-step reduction process: Nitrate is reduced to nitrite in the cytosol, and subsequently nitrite is reduced to ammonium in the chloroplast (Crawford et al. 2000). Reduced ferrodoxin is required to reduce nitrite to ammonium (Crawford et al. 2000). Because ferrodoxin is only reduced by photosystem I, nitrite starts accumulating intracellularly when nitrite reduction to ammonium is interrupted at night (Guerrero et al. 1981). Internal nitrite accumulation is cytotoxic for plants. Higher plants can avoid nitrite accumulation by downregulating nitrate uptake in the dark (Campbell 1999; Crawford et al. 2000); this is not the case for phytoplankton, where nitrate uptake is a continuous process and cells actively excrete nitrite to avoid internal nitrite concentration buildup (Serra et al. 1978; Campbell 1999). Conversely, under nitrate-limiting conditions, phytoplankton can directly take up nitrite and use it as an alternative nitrogen source during the day (Cresswell and Syrett 1982; Collos 1998).

Theoretical models have long been used to investigate the coupled dynamics of nutrients and phytoplankton population dynamics (Legovic and Cruzado 1997; Klausmeier et al. 2004). These models allow for calibration of species-specific rates of nutrient uptake and conversion into population biomass, and thus help to identify the nutrient

* Corresponding author: Martino.Malerba@my.jcu.edu.au

requirements and utilization patterns for particular species. However, while phytoplankton models focusing on nitrate and phosphate have been studied for decades (Droop 1973; Lehman et al. 1975), the role of nitrite as a potential source of nitrogen has received relatively little attention. This represents a significant knowledge gap. Although the experimental designs of these earlier studies likely prevented appreciable nitrite accumulation, models not accounting for nitrite release and uptake dynamics have the potential to produce biased estimates for rates of nitrogen assimilation and population growth, when applied to cases for which considerable nitrite buildup can occur in the medium (Collos 1998).

To date, the only model of phytoplankton dynamics that explicitly incorporates both nitrate and nitrite dynamics is the nitrite–ammonium–nitrate interaction model (NANIM), proposed by Flynn and Flynn (1998). NANIM is a highly complex model of nitrogen dynamics, containing mechanistic components simulating the most important biochemical pathways in phytoplankton physiology (nitrite reductase, glutamine pool, glutamine synthetase, amino acid pool, nitrogen quota, chlorophyll quota, etc.). Because of its focus on the roles of particular biochemical pathways, NANIM includes nine state variables and > 35 parameters. Consequently, calibrating this model for a particular species would require extremely large data sets, including detailed observations on several aspects of biochemistry, as well as on light regimes, chemical composition of the culture medium, and phytoplankton biomass. Furthermore, our knowledge of phytoplankton physiology is currently too limited to validate some assumptions of this model (e.g., presence of specialized nitrite uptake sites on cell surfaces; Galván and Fernández 2001). Thus, while NANIM can provide important qualitative insights into the biochemical mechanisms underpinning nitrite–phytoplankton dynamics, a simpler, more tractable framework, which can be more readily calibrated with experimental data, is also needed if we are to quantify how different nitrite utilization patterns affect the dynamics of different phytoplankton species.

The aim of this study was to design a model of phytoplankton growth that could be calibrated from time-series of readily measurable state variables. Specifically, our goal was to formulate a model with sufficiently few parameters to allow calibration from relatively short time-series of phytoplankton biomass and extracellular concentrations of nitrate and nitrite. To achieve this, we extended the "quota" modeling approach (Legovic and Cruzado 1997) to incorporate both the release and uptake of nitrite. Then we calibrated the model with growth and nitrate and nitrite utilization data for four phytoplankton species, using contemporary approaches for fitting multivariate autoregressive models (Hilborn and Mangel 1997; Bolker 2008). This relatively simple model successfully captures a broad range of qualitatively different nitrate and nitrite dynamics, and provides insight into alternative explanations for nitrite utilization patterns that have been observed in previous work. Our approach provides a foundation for a more comprehensive understanding of the role of nitrite dynamics of phytoplankton in natural and engineered systems.

Model development—The so-called "Quota model" is commonly employed to describe phytoplankton biomass growth (B) driven by extracellular nitrate (NO_3^-) and phosphate (PO_4^{3-}) concentrations (Klausmeier et al. 2004; Smith and Yamanaka 2007). In the present experiment, medium phosphate was oversupplied, and did not seem to limit growth rate (data not shown). Consistent with this, in preliminary fits of a version of our model that included phosphate limitation, most of the phosphate parameters had wide confidence intervals, and were in particular consistent with no effect of phosphate on population growth. Therefore, here we focus on the role of nitrogen. Although we assume that phosphate does not constrain cell division in our study populations, extension of the model to incorporate phosphate is straightforward (Legovic and Cruzado 1997; Klausmeier et al. 2004).

Following Legovic and Cruzado (1997), we assume that the state variable $Q(t)$ (for quota) represents the total amount of nitrogen within a single cell. A cell's quota includes both inorganic nitrogen reserves (i.e., nitrate and nitrite) and cellular nitrogen-rich compounds (e.g., pigments, Rubisco, etc.). $Q(t)$ increases as nitrate and nitrite are taken up. Nitrogen for cell division is supplied from this internal quota, so the rate of cell division ranges from zero, when the cell quota is at minimum level q_0, to a maximum of μ_{MAX} as $Q(t) \to \infty$. However, in contrast to Legovic and Cruzado (1997), we allow internal nitrogen concentration to increase due to uptake of nitrite, as well as nitrate. Hence, in our model internal nitrogen concentration decreases as excess nitrogen is released as nitrite, as well as when it is used for cell division.

Rather than attempting to capture oscillations in nitrite utilization between day and night phases due to an incomplete reduction of nitrate during the night (Collos 1998; Crawford et al. 2000), we are interested in the overall balance of medium nitrite as an average over the diurnal cycle. Therefore, medium nitrite was measured at the same time of the day, to ensure that any diurnal oscillations would not bias model parameters (*see* Methods). Thus, when internal nitrogen stores are full, nightly nitrite release will tend to exceed daily uptake, leading to an increase in medium nitrite concentration; conversely, as nitrate availability becomes limiting, daily nitrite uptake will tend to exceed nightly release, leading to depletion of nitrite from the medium. Specifically, we modeled the system dynamics as follows (*see* Table 1 for definitions):

$$\frac{d\mathrm{NO_3}(t)}{dt} = (a_{\mathrm{in}} \times \mathrm{NO_{3,in}} - b_{\mathrm{out}} \times \mathrm{NO_3}(t)) - f_{\mathrm{NO_3}}(\mathrm{NO_3}(t)) \times B(t) \quad (1a)$$

$$\frac{d\mathrm{NO_2}(t)}{dt} = (a_{\mathrm{in}} \times \mathrm{NO_{2,in}} - b_{\mathrm{out}} \times \mathrm{NO_2}(t)) + f_{\mathrm{NO_B}}(\mathrm{NO_3}(t),\mathrm{NO_2}(t),Q(t)) \times B(t) - f_{\mathrm{NO_2}}(\mathrm{NO_3}(t),\mathrm{NO_2}(t)) \times B(t) \quad (1b)$$

Table 1. Summary table of model state variables and parameters.

State variables	Definition (units)
NO_3	Nitrate in medium (μmol NO_3^- L^{-1})
NO_2	Nitrite in medium (μmol NO_2^- L^{-1})
Q	Nitrogen quota (μmol N $cell^{-1}$)
B	Biomass (cell mL^{-1})
Parameters	**Definition (units)**
a_{in}	Input dilution rate in chemostat systems (d^{-1})
b_{out}	Output dilution rate in chemostat systems (d^{-1})
$NO_{3,in}$	Concentration of nitrate supply (μmol NO_3^- L^{-1})
$NO_{2,in}$	Concentration of nitrite supply (μmol NO_2^- L^{-1})
$v_{MAX\_NO_3}$	Maximum per-capita nitrate uptake rate (μmol NO_3^- $cell^{-1}$ d^{-1})
k_{NO_3}	Nitrate half-saturation constant (μmol NO_3^- L^{-1})
c	Conversion coefficient from nitrate to nitrite [μmol $NO_2^- \times (\mu$mol $NO_3^-)^{-1}$]. Set at $c=1$
β	Maximum proportion of per-capita nitrate and nitrite uptake released as nitrite ($0 \le \beta \le 1$) (dimensionless)
$v_{MAX\_NO_2}$	Maximum per-capita nitrite uptake rate (μmol NO_2^- $cell^{-1}$ d^{-1})
φ	Nitrate inhibition for nitrite uptake (μmol NO_3^- $L^{-1})^{-1}$
k_{NO_2}	Nitrite half-saturation constant (μmol NO_2^- L^{-1})
q_0	Per-capita minimum nitrogen quota (μmol N $cell^{-1}$)
Q_{init}	Per-capita initial nitrogen quota (μmol N $cell^{-1}$)
μ_{MAX}	Growth rate at infinite nutrient storage (d^{-1})

$$\frac{dQ(t)}{dt} = f_{NO_3}(NO_3(t)) - f_{NO_B}(NO_3(t), NO_2(t), Q(t)) + f_{NO_2}(NO_3(t), NO_2(t)) - f_Q(Q(t)) \times Q(t) \quad (1c)$$

$$\frac{dB(t)}{dt} = -b_{out} \times B(t) + f_Q(Q(t)) \times B(t) \quad (1d)$$

$$f_{NO_3}(NO_3(t)) = v_{MAX\_NO_3} \times \frac{NO_3(t)}{NO_3(t) + k_{NO_3}} \quad (1e)$$

$$f_{NO_B}(NO_3(t), NO_2(t), Q(t)) = \beta \times (c \times f_{NO_3} + f_{NO_2}) \times \left(1 - \frac{q_0}{Q(t)}\right) \quad (1f)$$

$$f_{NO_2}(NO_3(t), NO_2(t)) = v_{MAX\_NO_2} \times e^{(-\varphi \times NO_3(t))} \times \frac{NO_2(t)}{NO_2(t) + k_{NO_2}} \quad (1g)$$

$$f_Q(Q(t)) = \mu_{MAX} \times \left(1 - \frac{q_0}{Q(t)}\right) \quad (1h)$$

The first term in Eq. 1a represents the increase in external nitrate concentration through supply, for example via upwelling or experimental addition, and the decrease as it flows out of the system without being assimilated; the second term represents the rate of medium nitrate decrease due to uptake and intracellular storage. The per-cell rate of nitrate uptake is modeled as a saturating function: Uptake increases with external concentration until the cell reaches its maximum uptake capacity ($v_{MAX\_NO_3}$ in Eq. 1e). The first term in Eq. 1b describes the increase and decrease of nitrite as it enters and leaves the system (e.g., through the inflow and outflow of a chemostat system); the second term represents the increase of nitrite as it is released by algal cells due to excess availability of nitrate in the external environment, while the third term describes nitrite uptake from the environment when nitrate is scarce.

The per-capita rate of nitrite release (f_{NO_B}) is modeled proportional to the per-capita nitrate + nitrite uptake and the available internal nitrogen quota, with c as the conversion coefficient from nitrate to nitrite ($c = 1$), and β as the maximum proportion of nitrite release constrained between 0 (no release) and 1 (nitrite release approaches nitrate + nitrite uptake as $Q(t) \to \infty$; Eq. 1f). Our rationale for modeling nitrite release in this way is that nitrate reduction is a light-independent process that is promptly carried out in the cytosol via transfer of electrons from nicotinamide adenine dinucleotide (NADH) to nitrate (Crawford et al. 2000). In contrast, nitrite reduction is a light-driven process that occurs exclusively through the provision of reduced ferrodoxin via photosystem I activity (Crawford et al. 2000). Thus, our functional response for nitrite release ensures that this process has a maximum rate of $\beta \times (c \times f_{NO_3} + f_{NO_2})$, which cannot be greater than its total inorganic nitrogen uptake (i.e., $0 \le \beta \le 1$), and will be approached only when nitrogen cellular stores have been filled (Eq. 1f). In principle, nutrient uptake and release parameters could vary depending on light conditions (Mackey et al. 2011), and therefore parameter values for any given species should be interpreted as specific to the light regime under which the model is calibrated. However, the model in Eq. 1 could readily be generalized to incorporate light-dependent uptake and release, by calibrating functional relationships between these parameters and irradiance levels.

Table 2. Clone number and dry weight estimates (g dry wt mL^{-1}) employed for inoculation for all four species.

Species	Clone number	Dry weight (±1 SE)
Picochlorum atomus	NQAIF 284	$1.41\times10^{-8}(\pm5.50\times10^{-9})$
Nannochloropsis oculata	NQAIF 283	$2.94\times10^{-9}(\pm1.19\times10^{-9})$
Isochrysis sp.	NQAIF 001	$8.60\times10^{-9}(\pm3.31\times10^{-9})$
Pyrocystis lunula	NQAIF 016	$1.11\times10^{-5}(\pm4.17\times10^{-6})$

In the absence of other nitrogen sources, nitrite uptake is modeled to be greatest ($v_{MAX\_NO_2}$) in nitrate-free environments, and to decrease exponentially with increasing extracellular nitrate concentration, with φ as the coefficient quantifying the effect of nitrite uptake on nitrate concentration (Eq. 1g). Our rationale for this functional form is that the nitrogen source supplied to the culture prior to the experiment predisposes cells to different degrees of uptake inhibition for alternative nitrogen forms (Dortch 1990; Dortch et al. 1991). The model predicts nitrite utilization to increase from negligible to substantial when medium nitrate concentrations are depleted. This is commonly observed in previous experiments on nitrate-reared batch cultures (Cresswell and Syrett 1982).

The per-cell internal nitrogen quota $Q(t)$ increases as nitrate and nitrite are taken up, and decreases as nitrogen is expelled as nitrite or is used for population growth (Eq. 1c). Our experimental setting did not require the specification of an upper bound for $Q(t)$, as internal nitrogen is the only resource regulating growth rate. This implies that $Q(t)$ will always tend toward an equilibrium state, defined by μ_{MAX}, nitrogen uptake, and q_0, where nitrogen uptake equals nitrogen costs for cell division. Under other circumstances, however, extension of the model to incorporate a maximum value of $Q(t)$ could be necessary. For instance, in the case of multiple limiting nutrients, the current model formulation could predict unbounded accumulation of internal nitrogen when the other nutrient is limiting population growth. Finally, utilization of stored nitrogen for population growth follows a rectangular hyperbola, characterized by a maximum rate of biomass production (μ_{MAX}) and a minimum internal nitrogen concentration (q_0) at which cell division ceases (Eq. 1h).

Note that, because all parameters present in Eq. 1c also appear in one of the other equations, it was possible to calibrate the model using only observations on phytoplankton biomass, and external nitrite and nitrate concentrations, and to infer the internal nitrogen dynamics from the fitted parameter values.

Methods

Culture maintenance—Monoclonal cultures of *Picochlorum atomus* (Butcher) (Chlorophyta), *Nannochloropsis oculata* (Droop) (Ochrophyta), *Isochrysis* sp. (Haptophyta), and *Pyrocystis lunula* (Schütt) (Dinophyta) were selected for experimental evaluation of growth and nitrate and nitrite utilization (*see* Table 2 for culture accession numbers); the species were chosen to offer a broad range of cell sizes and taxonomic diversity (*see* Table 2 for species dry weight). Cultures were sourced from the North Queensland Algal Culturing and Identification Facility (NQAIF) at the School of Marine and Tropical Biology at James Cook University, Townsville, Australia.

All cultures used for experiments were maintained in L1 medium (Harrison and Berges 2005) prepared with filtered seawater (0.45-μm High Vacuum Durapore, Millipore) in a temperature-controlled phytoplankton room at 24°C and a 12 : 12 light : dark photoperiod in the Biological Sciences Building at the James Cook University (Townsville, Australia). Mother cultures were maintained at NQAIF in Contherm cross-flow phytoplankton growth chambers (Contherm Scientific Limited) using the same medium, temperature, and lighting conditions. Light was provided by cool-white fluorescent lights at a photon flux density of 42 μmol photons m^{-2} s^{-1}. All culturing materials were autoclaved and handled aseptically in a laminar flow cabinet (Alternative Environmental Solutions fitted with High-Efficiency Particulate Arresting filter, Australia Standards 4260, National Association of Testing Authorities certified).

Experimental design—Due to differences in species size, the starting inoculation was standardized across species using biomass dry weight (g dry wt mL^{-1}). Three replicate cultures were inoculated with 0.00146 g dry wt mL^{-1} per species, and growth and nitrate and nitrite utilization were monitored over a period of 21 d in 500-mL cultures for *Isochrysis* sp. and *Nannochloropsis oculata*, 9 d in 500-mL cultures for *Picochlorum atomus* and 13 d in 1-liter cultures for *Pyrocystis lunula*. A total sample volume of 6.75 mL was removed daily from each culture for *Isochrysis* sp., *Nannochloropsis oculata*, and *Picochlorum atomus*: 3 × 250 μL was used for estimating cell concentration, and 6 mL was used for analysis of culture medium nitrate and nitrite. For *Pyrocystis lunula*, the total sample volume was 11 mL per replicate culture, as the sample volume required for three manual cell counts was 5 mL.

Estimation of culture cell concentration—Total cell number was determined by direct cell count and indirectly using turbidity (percent optical transmission at 750 nm) for *Nannochloropsis oculata*, *Isochrysis* sp., and *Picochlorum atomus*; *Pyrocystis lunula* could only be counted directly due to rapid sedimentation caused by its large cell size.

Methods for indirect optical transmission were adapted from Harrison and Berges (2005). A volume of 250 μL of culture was loaded on a 96-well microtiter plate (Ultraviolet-Star®, Greiner Bio-One GmbH) and percent transmission at 750 nm was measured on a SpectraMax® Plus384 (Molecular Devices). To establish calibration curves indirect proxy culture turbidity (percent transmission) was correlated with direct cell counts per milliliter in Statistica 8

(Statsoft®) with a second-order polynomial curve fit ($R^2 > 0.98$).

Direct cell counts for *Isochrysis* sp., *Nannochloropsis oculata*, and *Picochlorum atomus* for establishment of calibration curves were carried out on a Neubauer Improved haemocytometer under ×40 magnification on a Leica high-resolution microscope. For total cell number estimation of *Pyrocystis lunula*, 5-mL samples were taken daily from each culture replicate, fixed with Lugol's iodine (Throndsen 1978) at a final concentration of 2%. Cells were counted in a 1-mL Pyser Sedgewick Rafter under ×10 magnification with a Leica high-resolution microscope.

Dry weight—Twenty-five-millimeter glass fiber filters (pore size 1.2 μm, Millipore, Sigma-Aldrich) were pre-combusted on aluminum foil squares (10 cm × 10 cm) using a muffle furnace at 400°C for 10 h. Filters were weighed prior to sample filtration. After filtration of one 10-mL sample per species, each filter was dried in a drying oven at 100°C overnight. After cooling for 30 min, filters were weighed. The weight of each filter prior to filtration was subtracted from this weight. All dry weights were corrected for salt content by subtracting the mean weight of the same volume of medium without cells (salt blanks). The mean weight of a cell was calculated from measurements of dry weight and cell density for five differently concentrated culture samples per species.

Nutrient analyses—All chemicals for culturing and nutrient analyses were purchased from Sigma-Aldrich unless stated otherwise. Six milliliters of culture was centrifuged at 3000 × *g* at 20°C for 20 min (Eppendorf R 5810). Five milliliters of supernatant was filtered through cellulose acetate syringe filters (0.45 μm, Satorius Stedein Biotech GmbH), referred to as culture supernatant hereafter; from the 5 mL of culture supernatant 1.25 mL were used for each nitrate (NO_3^-) and nitrite (NO_2^-) analyses. For each species, nitrate and nitrite concentrations were analyzed using one sample per replicate culture ($n = 3$ independent between culture replication).

Analysis of nitrate (NO_3^-) and nitrite (NO_2^-)—Nitrate and nitrite assays were performed as per Carvalho et al. (1998). Measurements of medium nitrate and nitrite were conducted every day 3 h into the day phase, in order to control for any diurnal fluctuations in nitrate and nitrite, and thus more clearly capture the longer-term trends. In other words, by measuring nitrite and nitrate at the same time every day, parameter estimates were not biased by diurnal fluctuations in those variables.

The nitrite assay required three solutions for the colorimetric determination of nitrite concentration: (1) 1 L containing 13 g of NH_4Cl, 1.7 g ethylenediaminetetraacetic acid adjusted to pH 8.5 with 28% NH_4Cl; (2) 5 g of sulfanilamide in 300 mL of acidified deionized water (HCl final concentration of 5.29%); (3) 500 mg of *N*-(1-naphtyl)-ethylenediamine in 500 mL of deionized water. All glassware was acid washed (10% HCl). A sample of 1.25 mL of filtered culture supernatant was mixed with 3.75 mL of solution 1 and 200 μL of solution 2. After 5 min of reaction time, 200 μL of solution 3 was added. Samples were thoroughly vortexed after addition of each reagent. After 10 min, 250 μL was transferred onto a 96-well-plate (Iwaki®, Barloworld Scientific) and absorbance was measured at 540 nm (SpectraMax® Plus384).

Medium nitrate + nitrite was analyzed by adding 25 μL 1 mol L^{-1} HCl to 1.25 mL of filtered culture supernatant. After vortexing, 250 μL was transferred onto a 96-well-plate (Ultraviolet-Star®, Greiner Bio-One GmbH) and absorbance was recorded at 220 nm (SpectraMax® Plus384). Nitrate concentration was calculated by subtracting the medium nitrite concentration from the medium nitrate + nitrite measurements, as both nitrate and nitrite absorb at 220 nm. Standard curves for both nitrate and nitrite were kindly supplied by NQAIF. Filtered seawater with reactants for nitrite and nitrate analyses were used as blanks to zero the spectrophotometer.

Model calibration—Model parameters and (where appropriate) initial conditions for state variables were estimated by maximum likelihood methods. To estimate model parameters with likelihood techniques, we first obtained the deterministic component of the model by discretizing the continuous-time formulation of Eq. 1, following standard procedures (Turchin 2003). Discretization can occasionally produce qualitative artifacts in dynamics, for instance by introducing population cycles not present in the continuous-time formulation, due to the implicit lag of one time step. To confirm that this was not happening in our case, we used our parameter estimates to simulate the dynamics of both the original continuous time model (using package deSolve in R; Soetaert et al. 2010), and the deterministic component of the discrete-time model, and we compared the resulting trajectories.

To constrain all measured values (cell number and nutrient concentrations) to be nonnegative, we assumed a log-normal error distribution. The right-skewed nature of this distribution allows for occasional very large positive residuals, which are often observed in population data. The appropriate form of the likelihood function depends upon whether the deviations between observed and predicted values are dominated by process error (i.e., differences due to stochasticity in the culture dynamics itself), or by observation error (i.e., differences between observed and predicted values due to measurement error). Specifically, the negative log-likelihood function accounting for process error ($-L_{\text{pro,t}}$) calculates the state of the system at time t depending on the observed state at time $t - 1$ as:

$$\begin{aligned} -L_{\text{pro,t}}\{\mathrm{Y}_{\text{obs,t}}|f(\mathrm{Y}_{\text{obs,t}-1}),\Sigma_{\text{pro}}\} &= \\ n\left[\frac{1}{2}\log\left\{\det\left(\sum\nolimits_{\text{pro}}\right)\right\}+\frac{d}{2}\log(2\pi)\right] & \\ +\frac{1}{2}\{\log(\mathrm{Y}_{\text{obs,t}})-\log[f(\mathrm{Y}_{\text{obs,t}-1})]\}^{\mathrm{T}}\sum\nolimits_{\text{pro}}^{-1}\{\log(\mathrm{Y}_{\text{obs,t}}) & \\ -\log[f(\mathrm{Y}_{\text{obs,t}-1})]\} & \end{aligned} \tag{2}$$

where $d = 3$ is the number of dimensions of the observed data (i.e., population size, nitrate and nitrite concentration),

n is the number of observations (i.e., the length of the time series), Σ_{pro} is the $d \times d$ variance–covariance matrix (with variances along the diagonal and covariances in the off-diagonal elements), and $Y_{obs,t}$ and $f(Y_{obs,t-1})$ are two $d \times n$ matrices containing observed values at time t and model-predicted values (from the discretization of Eq. 1) based on the observed state of the system at time $t - 1$, respectively. In contrast, the negative log-likelihood function accounting for observation error ($-L_{obs,t}$) predicts state variable values at time t from the model's predicted value at the previous time:

$$\begin{aligned} &-L_{obs,t}\left\{Y_{obs,t}\middle|f(Y_{pred,t-1}),\Sigma_{obs}\right\} = \\ &n\left[\frac{1}{2}log\left\{\det\left(\sum{}_{obs}\right)\right\}+\frac{d}{2}log(2\pi)\right] \\ &+\frac{1}{2}\left\{log(Y_{obs,t})-log\left[f(Y_{pred,t-1})\right]\right\}^{T}\sum{}_{obs}{}^{-1}\left\{log(Y_{obs,t})\right. \\ &\left.-log\left[f(Y_{pred,t-1})\right]\right\} \end{aligned} \tag{3}$$

where $f(Y_{pred,t-1})$ is a $d \times n$ matrix with model-predicted values calculated from the predicted state of the system at time $t - 1$ (according to the discretization of Eq. 1), and Σ_{obs} is a $d \times d$ variance–covariance matrix.

In the observation-error model, the off-diagonal elements of Σ_{obs} (covariance between residuals of population size, nitrate, and nitrite) are constrained to be zero because measurements for nitrate, nitrite, and population size were made independently, and thus residuals are caused by independent measurement uncertainties. This contrasts with the process-error likelihood, because the process-error formulation attributes residual variation to stochasticity in the culture system itself, so statistical covariances among residuals would be expected to arise from the dynamic coupling between population size and nutrient concentration (Petersen and Pedersen 2008). For example, if population growth is unusually large for a particular day (producing a positive residual in population size), then nitrate concentration may well be expected to decrease more than predicted (i.e., exhibit a negative residual), to account for the nutrients required for the excess cell proliferation.

Although, in principle, it is possible to formulate a likelihood that accounts simultaneously for process and observation error, such approaches require hundreds of observations, far beyond what is generally available in biological time series (Dennis et al. 2010). Instead, we follow an approach commonly used in population time series: We fit process- and observation-error likelihood functions separately, and assess the robustness of parameter estimates by comparing the fits of the two different statistical models (Hilborn and Mangel 1997).

Maximum log-likelihoods and maximum likelihood parameter estimates were obtained by using the optimization function nlminb() in the software program R (R Development Core Team 2011). Profile likelihood intervals were used to obtain 95% confidence intervals on the parameter estimates. Because we employed batch-culture systems, there was no external exchange of nitrate during the course of the experiments. Therefore, the rates of nutrient supply and removal, a_{in} and b_{out}, were fixed at zero in all analyses. Note also that, for process-error models, initial values of observed state variables ($NO_{3,init}$, $NO_{2,init}$, and B_{init}) are taken to be the observed initial values, and thus are not estimated (Hilborn and Mangel 1997).

Model selection—Since the populations analyzed in this study did not reach stationary growth phase (*see* Results) and only one species exhibited both medium nitrite increase and decrease, there were often insufficient data to obtain good estimates of all parameters in the model. Therefore, we also fitted simplified versions of the model, with particular parameters set at limiting values, and we used formal model selection with Akaike Information Criterion (AIC; Bozdogan 1987) to determine which parameters to retain in the final model for each species. Specifically, we removed single and combinations of parameters from the fully parameterized form of each functional response (i.e., f_{NO_3}, f_{NO_B}, and f_{NO_2}) and determined through AIC scores the model best-fit, leaving the remaining functional responses fully parameterized.

Model cross-validation—As a further check against overfitting, and to assess the model's ability to predict data not used in model fitting (i.e., its capacity for out-of-sample prediction), we carried out cross-validation analyses. Because we reared three independent cultures, a straightforward way to cross-validate the model was to calibrate it with two cultures (i.e., training cultures), and calculate the coefficient of determination (R^2) between the resulting model predictions and the corresponding observed values from the third culture (i.e., validating culture; Turchin 1996; Cusson and Bourget 2005). We repeated the cross-validation three times per species, using all possible combinations of two training and one validating cultures. We then calculated aggregate R^2 prediction error (R^2_{pred}) scores for each state variable as follows:

$$R^2_{pred} = 1 - \frac{\sum_{c=1}^{3}\sum_{i=1}^{n}\left(y_{c,i}-\hat{y}_{-c,i}\right)}{\sum_{c=1}^{3}\sum_{i=1}^{n}\left(y_{c,i}-\bar{y}_{c}\right)} \tag{4}$$

where c indexes the culture (1, 2, or 3), i indexes the observations within each culture, n is the number of observations per culture (i.e., the number of days on which measurements were made), $y_{c,i}$ is the observed value from culture c on day i, $\hat{y}_{c,i}$ is the predicted value from calibrating the model to the other two cultures (i.e., excluding culture c), and $\bar{y}_c$ is the mean of the observed values from culture c (Kutner et al. 2004).

To compare these model fit statistics with an index of total explained variability from the original fits, we also calculated R^2 residual (R^2_{resid}) error in the standard way:

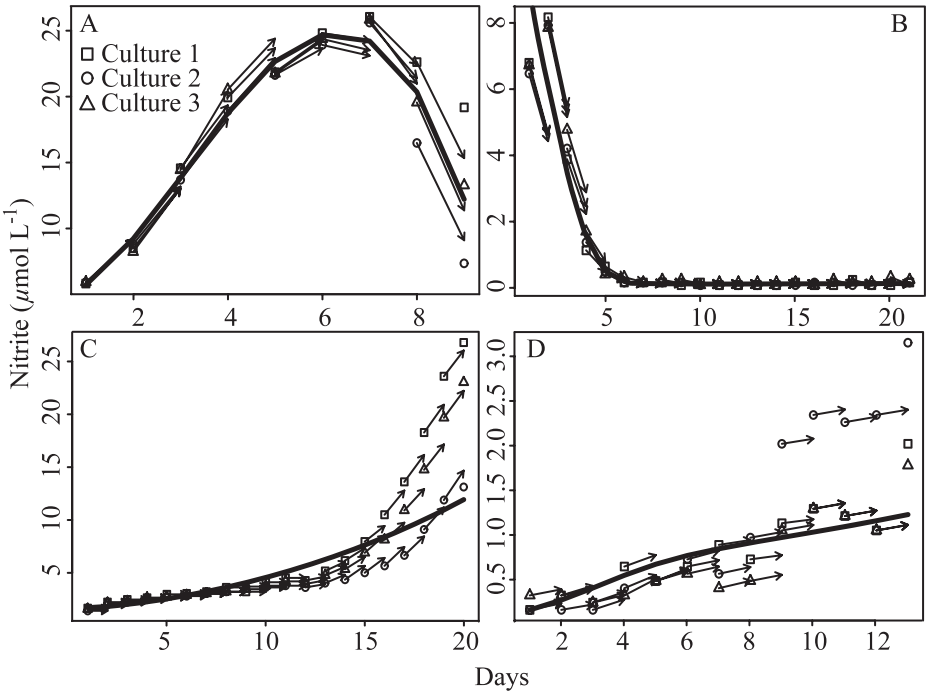

Fig. 1. Medium nitrite dynamics for (A) *Picochlorum atomus*, (B) *Nannochloropsis oculata*, (C) *Isochrysis* sp., and (D) *Pyrocystis lunula*. The different symbols show the observed data for the three replicate cultures per species. The solid line shows the best-fit model with observation error. Because this model assumes that the noise in the data is dominated by observation error, predicted values at time $t + 1$ are calculated from the predicted values at time t, and thus the best-fit trajectory is a smooth line. The arrows show the best-fit model with process error. Because the process-error model assumes that the noise is dominated by real biological variability, the observed values at time t (base of the arrows) are used to obtain predict values at time $t + 1$ (arrowheads; "one-step ahead" prediction: *see* Bolker 2008).

$$R^2_{\text{resid}} = 1 - \frac{\sum_{c=1}^{3}\sum_{i=1}^{n}(y_{c,i} - \hat{y}_i)}{\sum_{c=1}^{3}\sum_{i=1}^{n}(y_{c,i} - \bar{y}_c)} \quad (5)$$

where $\hat{y}_i$ is the predicted value based on the residuals of the model fitted to all three replicate cultures simultaneously. For each fit the prediction R^2 can only be equal to or less than the R^2 residual score; the closer the two scores are to one another, the more accurate are the model's out-of-sample predictions.

Results

Culture dynamics—Fits of the model to the data suggest that the model successfully captured the broad range of culture medium nitrite utilization patterns exhibited by the four different species (Fig. 1). For *Picochlorum atomus*, culture medium nitrite concentration showed an initial period of increase followed by depletion from day 6 onward (Fig. 1A). For *Nannochloropsis oculata*, net release of nitrite was observed only between the first and second day of the culture period, followed by rapid depletion until the medium was almost completely nitrite-deplete by day 6 (Fig. 1B). However, this short initial release was not captured by the model, which predicted gradual net nitrite uptake throughout. In contrast, culture medium nitrite increased monotonically for *Isochrysis* sp. and *Pyrocystis lunula* over the culture period (Fig. 1C,D).

The model captured changes in population growth for all species (Fig. 2). Excluding *Isochrysis* sp., which showed approximately exponential growth (Fig. 2C: Note approximate linearity on the logarithmic scale after the first few days, indicating exponential growth), all other species displayed growth profiles characterized by two phases of growth: An initial rapid culture growth lasting from 3 to 5 days, followed by a second phase of slower growth (Fig. 2A,B,D). The model associated the decrease in growth rate with a reduction in internal nutrient availability: The biphasic growth profiles for *Picochlorum atomus*, *Nannochloropsis oculata*, and *Pyrocystis lunula* were explained by the model with an initially high internal nutrient status followed by partial intracellular nitrogen storage depletion (Fig. 3A,B,D). Since population growth was approximately exponential for *Isochrysis* sp., model parameters implied that cultures were not limited in internal nitrogen at any time during the experiment (increasing internal quota, Fig. 3C).

Medium nitrate depletions were the only dynamics showing clear evidence of systematic deviation from the fitted models (Fig. 4). While the model described the

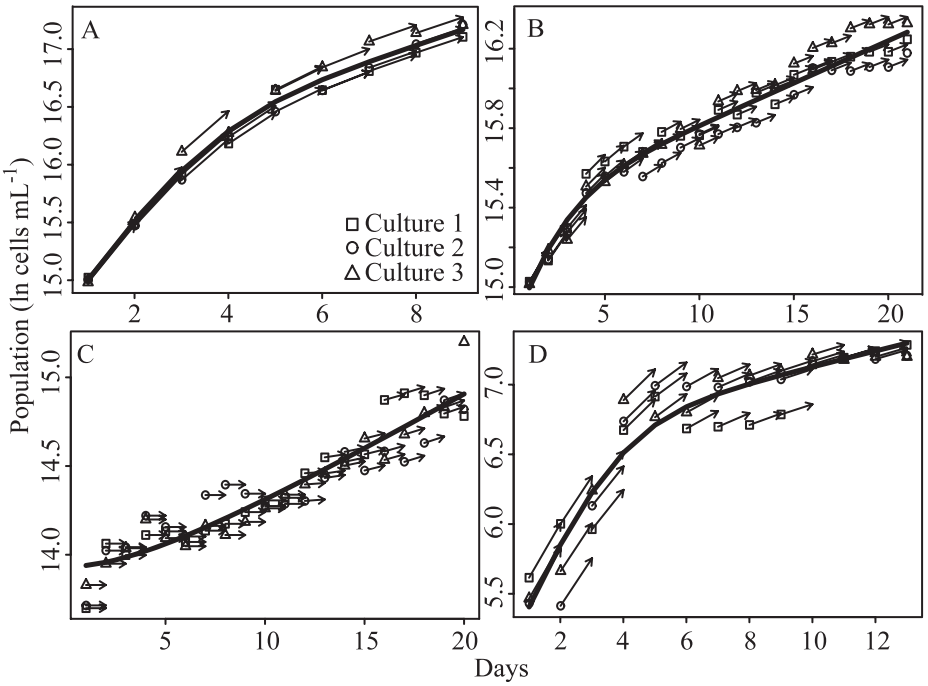

Fig. 2. Population growth (log-transformed) for (A) *Picochlorum atomus*, (B) *Nannochloropsis oculata*, (C) *Isochrysis* sp., and (D) *Pyrocystis lunula*. The different symbols show the observed data for the three replicate cultures per species. The solid line shows the best-fit model with observation error. Arrows show the best-fit model with process error. *See* Fig. 1 legend for a detailed description of observation- and process-error model fitting.

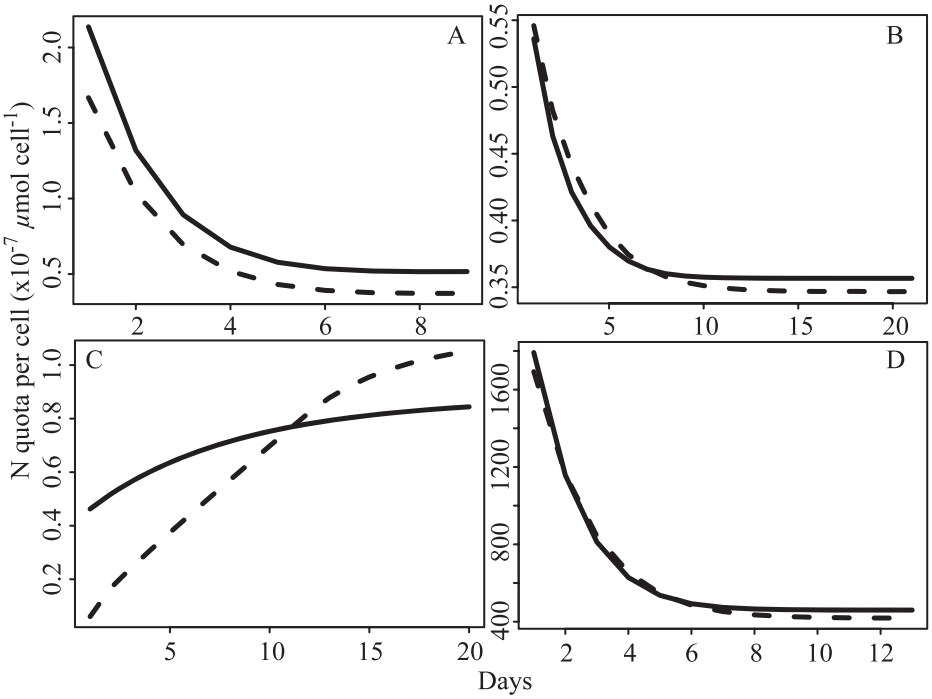

Fig. 3. Internal nitrogen quota for (A) *Picochlorum atomus*, (B) *Nannochloropsis oculata*, (C) *Isochrysis* sp., and (D) *Pyrocystis lunula* inferred from the observation-error (solid line) and process-error (dashed line) likelihoods. Note that, because there were no direct observations of internal quota levels, predicted trajectories for both likelihoods are generated using the estimates of initial quota levels obtained from the respective maximum likelihood fits (refer to Table 5).

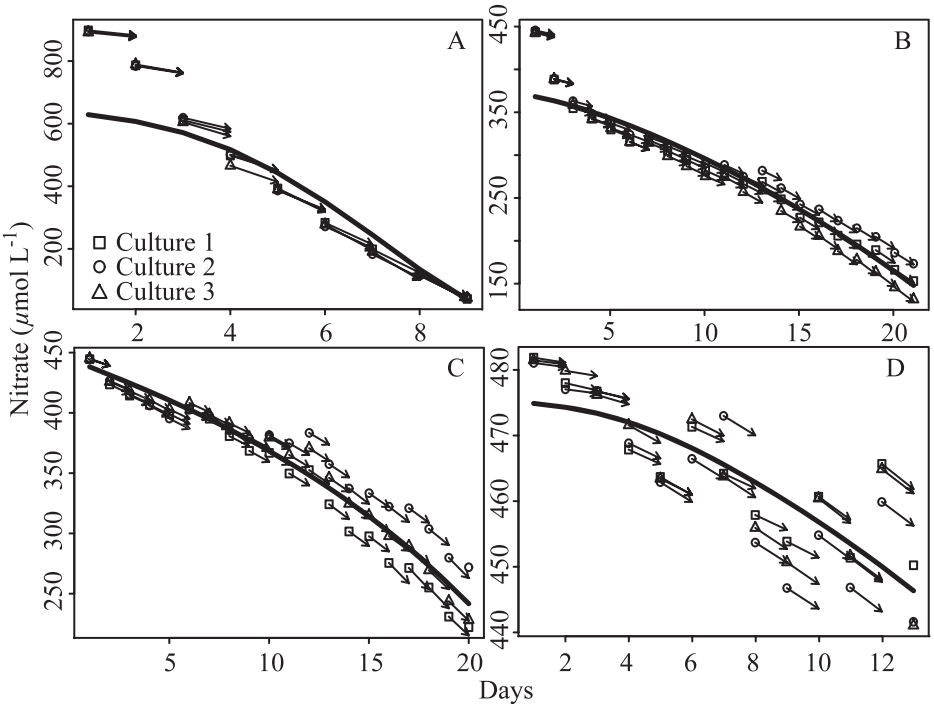

Fig. 4. Medium nitrate dynamics for (A) *Picochlorum atomus*, (B) *Nannochloropsis oculata*, (C) *Isochrysis* sp., and (D) *Pyrocystis lunula*. The different symbols show the observed data for the three replicate cultures per species. The solid line shows the best-fit model with observation error. Arrows show the best-fit model with process error. *See* Fig. 1 legend for a detailed description of observation- and process-error model fitting.

broad-scale features of nitrate uptake relatively well, it did not capture the initially high nitrate consumption in *Picochlorum atomus* or *Nannochloropsis oculata* during the first 3 and 2 d of the culture period, respectively (i.e., the rapid initial decline in observed nitrate values; Fig. 4A,B). This is apparent in the observation-error fit by the model's underprediction of nitrate levels early in the experiment (solid lines in Fig. 4A,B), and in the process-error fit by the model's tendency to underestimate the magnitude of decline in nitrate in the first few days of the experiment (arrows in Fig. 4A,B). In contrast, nitrate depletion for *Isochrysis* sp. (Fig. 4C) and *Pyrocystis lunula* (Fig. 4D) showed little evidence of systematic discrepancies between the model and the data.

Cross-validation analysis yielded a total of 12 prediction R^2 scores (4 species $\times$ 3 state variables), for both observation- and process-error models. For eight of the 12 observation-error cases, and all of the process-error cases, prediction R^2 values were within 5% of the residual R^2 scores (Table 3), indicating very good predictive ability of the models. Also, all parameter estimates from all combinations of training sets fell within the 95% confidence intervals of the estimates obtained from the original analysis (data not shown).

Model comparisons—According to AIC, the best-fitting model included all nitrite-related parameters (β, $v_{MAX\_NO_2}$, and φ) only when the data displayed both periods of net release and uptake (i.e., *Picochlorum atomus*; Table 4). *Nannochloropsis oculata* cultures showed little net nitrite release, so model selection favored a model omitting this process (β fixed at 0; Table 4). Also, *Nannochloropsis oculata* was the only species showing evidence of a reduction in per-capita nitrite uptake due to resource limitation; therefore, it was the only species whose best-fitting model included the nitrite half-saturation constant (k_{NO_2}; Table 4). *Pyrocystis lunula* and *Isochrysis* sp. cultures did not exhibit net nitrite depletion during any stage of the experiment, so the model with no nitrite uptake ($v_{MAX\_NO_2}$ and φ set to zero) was therefore favored by AIC (Table 4). Finally, since none of the species exhibited nitrate-limited uptake dynamics, there was little information in the data to estimate half-saturation constants in the Michaelis–Menten saturating functions, and thus model selection favored modeling nitrate uptake at a constant per-cell rate (i.e., $k_{NO_3} = 0$; Table 4).

Parameter estimates obtained from the two distinct process-error and observation-error likelihoods were overall quite consistent (Table 5). The two sets of parameters were particularly similar in *Pyrocystis lunula*, with all values within 5–30% of each other and very substantial overlap in the models' respective 95% confidence limits (Table 5). Similarly, parameter estimates for *Nannochloropsis oculata* showed good consistency. There was a relatively large (2.5-fold) difference in the nitrite half-saturation constant (k_{NO_2}); however, this was due to the very broad confidence limits on this parameter in both models, rather than to a systematic discrepancy between the models (Fig. 1B; Table 5). Parameter estimates for *Picochlorum atomus* when calibrated with the observation-

Table 3. Coefficients of determination (R^2) from the cross-validation analyses for the three state variables for each of the four species using observation and process error calibrations. Squared residual error is denoted R^2_{resid} (Eq. 5), and squared cross-validation prediction error is denoted R^2_{pred} (Eq. 4).

	Observation error						Process error					
	Nitrite		Population		Nitrate		Nitrite		Population		Nitrate	
	R^2_{resid}	R^2_{pred}	R^2_{resid}	R^2_{pred}	R^2_{resid}	R^2_{pred}	R^2_{resid}	R^2_{pred}	R^2_{resid}	R^2_{pred}	R^2_{resid}	R^2_{pred}
Picochlorum atomus	0.91	0.82	0.97	0.95	0.83	0.83	0.93	0.91	0.97	0.97	0.94	0.94
Nannochloropsis oculata	0.94	0.94	0.94	0.89	0.92	0.90	0.86	0.86	0.96	0.96	0.97	0.97
Isochrysis sp.	0.61	0.52	0.86	0.83	0.94	0.89	0.98	0.98	0.83	0.83	0.98	0.98
Pyrocystis lunula	0.41	0.35	0.89	0.84	0.67	0.65	0.79	0.79	0.85	0.85	0.39	0.39

error model were also fairly similar, except for nitrate uptake ($v\text{MAX\_NO}_3$, Table 5). This was mainly caused by the rapid uptake for the first 2 d (Fig. 4A): When the two nitrate uptake parameters were calculated excluding the first two observations, they were considerably more similar (5.71×10^{-9} [CI: 5.1–6.2 $\times 10^{-9}$] with observation-error model; 4.64×10^{-9} [CI: 4.1–5.3 $\times 10^{-9}$] with process-error model).

In contrast to the other three species, however, *Isochrysis* sp. showed considerable differences between the observation- and process-error-based parameter estimates (Table 5). While the values for nitrate uptake ($v\text{MAX\_NO}_3$) and maximum population growth (μ_{MAX}) were similar, maximum proportion of nitrite release (β) and internal quota (q_0 and Q_{init}) parameters were substantially different (Table 5). The model structure does not incorporate any mechanism that could explain the dynamics observed from day 1 to day 13, when exponentially dividing cells (Fig. 2C) did not release significant amounts of nitrite into the medium (Fig. 1C). Therefore, different compromises to account for this were reflected in observation- and process-error fits. Specifically, the observation-error fits captured exponential population growth (solid line in Fig. 2C), while substantially underpredicting nitrite release rates from day 13 onward (solid line in Fig. 1C). Conversely, the process-error fit matched the initially slow but later rapidly increasing nitrite release (arrows in Fig. 1C), while underpredicting initial population growth (arrows in Fig. 2C). The differences in internal nutrient dynamics reflect these different trade-offs (Fig. 3C). When the model predicts approximately exponential population growth together with constant nitrite accumulation (solid line in Figs. 1C, 2C), as in the observation-error model, the internal quota increased only slightly (solid line in 3C). In contrast, when the model predicts a late, rapid increase in both population growth and nitrite release (arrows in Figs. 1C, 2C), as in the process-error model, a larger increase (off a lower base) in the internal quota is implied (dashed line in Fig. 3C).

Discussion

Our results show that the nitrate–nitrite model developed in this study can characterize well the nitrite, nitrate, and biomass dynamics in four diverse phytoplankton species, even though those species display qualitatively different nutrient utilization patterns. This model mechanistically describes the coupled dynamics of biomass growth, extracellular nitrate and nitrite concentrations, and internal nitrogen quota. The advantages offered by this model are that it can be readily calibrated with time-series data and that it does not require explicit observations of internal nitrogen status. Moreover, by fitting the model in two different ways, one assuming that the variability in the data is driven mainly by observation error and another

Table 4. Formal model selection with AIC between functional responses for nitrate uptake (f_{NO_3}), nitrite release (f_{NO_B}), and nitrite uptake (f_{NO_2}). Values represent the difference in AIC (ΔAIC) scores (thus, by definition, the best fit model has ΔAIC = 0). Boldface indicates the estimated best-fitting model and therefore the one employed for parameter estimation. *See* Eq. 1e–g for full functional responses and Table 1 for parameter definitions.

			Picochlorum atomus	*Nannochloropsis oculata*	*Isochrysis* sp.	*Pyrocystis lunula*
f_{NO_3}	(1)	$v\text{MAX\_NO}_3 \times \frac{NO_3(t)}{NO_3(t)+k\text{NO}_3}$	2; 2	3; 4	2; 2	2; 2
	(2)	$v\text{MAX\_NO}_3 \times (NO_3(t)>0)$	**0; 0**	**0; 0**	**0; 0**	**0; 0**
f_{NO_B}	(1)	$\beta \times (c \times f_{NO_3} + f_{NO_2}) \times \left(1 - \frac{q_0}{Q(t)}\right)$	**0; 0**	2; 2	**0; 0**	**0; 0**
	(2)	0	63; 64	**0; 0**	107; 66	43; 26
f_{NO_2}	(1)	$v\text{MAX\_NO}_2 \times e^{(-\varphi \times \text{NO}_3(t))} \times \frac{NO_2(t)}{NO_2(t)+k\text{NO}_2}$	2; 2	**0; 0**	6; 6	6; 6
	(2)	$v\text{MAX\_NO}_2 \times e^{(-\varphi \times \text{NO}_3(t))} \times (NO_2(t)>0)$	**0; 0**	4; 16	4; 4	4; 4
	(3)	$v\text{MAX\_NO}_2 \times (NO_2(t)>0)$	5; 2	2; 18	2; 2	2; 2
	(4)	0	46; 64	75; 26	**0; 0**	**0; 0**

Table 5. Summary table (± 95% CI) for model parameters of each species calibrated with both observation- and process-error models. Profile likelihood intervals were used to obtain 95% confidence intervals on the parameter estimates. Number of parameters might differ between species due to simplification of functional responses selected through AIC model selection criteria (*see* Table 4). Consult Table 1 for definitions and units.

	Picochlorum atomus	
	Observation error	Process error
$v_{MAX\_NO_3}$	$6.7\times10^{-9}(5.9\times10^{-9}; 7.5\times10^{-9})$	$4.7\times10^{-9}(4.2\times10^{-9}; 5.3\times10^{-9})$
β	0.17(0.13; 0.24)	0.2(0.16; 0.25)
$v_{MAX\_NO_2}$	$1.1\times10^{-9}(6.5\times10^{-10}; 1.8\times10^{-9})$	$1\times10^{-9}(5.9\times10^{-10}; 1.4\times10^{-9})$
φ	$3.5\times10^{-3}(1.7\times10^{-3}; 7.0\times10^{-3})$	$4.3\times10^{-3}(2.1\times10^{-3}; 6.4\times10^{-3})$
μ_{MAX}	0.63(0.53; 0.75)	0.61(0.50; 0.69)
q_0	$4.0\times10^{-8}(3.3\times10^{-8}; 9.1\times10^{-8})$	$2.9\times10^{-8}(1.7\times10^{-8}; 1.0\times10^{-7})$
Q_{init}	$2.1\times10^{-7}(1.3\times10^{-7}; 5.3\times10^{-7})$	$1.7\times10^{-7}(8.3\times10^{-8}; 1.2\times10^{-6})$
	Nannochloropsis oculata	
$v_{MAX\_NO_3}$	$1.5\times10^{-9}(1.4\times10^{-9}; 1.6\times10^{-9})$	$1.4\times10^{-9}(1.2\times10^{-9}; 1.7\times10^{-9})$
$v_{MAX\_NO_2}$	$1.9\times10^{-9}(1.3\times10^{-9}; 3.7\times10^{-9})$	$2.6\times10^{-9}(1.5\times10^{-9}; 4.4\times10^{-9})$
k_{NO_2}	7.23(3.7; 16.1)	16(6.7; 19.5)
φ	1.5×10^{-8}(0; 0.05)	9.5×10^{-8}(0; 0.004)
μ_{MAX}	0.50(0.41; 0.68)	0.38(0.22; 0.58)
q_0	$3.2\times10^{-8}(3.1\times10^{-8}; 3.7\times10^{-8})$	$3.1\times10^{-8}(2.3\times10^{-8}; 6.9\times10^{-8})$
Q_{init}	$5.4\times10^{-8}(4.2\times10^{-8}; 1.8\times10^{-7})$	$5.5\times10^{-8}(3.1\times10^{-8}; 1.3\times10^{-7})$
	Isochrysis sp.	
$v_{MAX\_NO_3}$	$6.0\times10^{-9}(5.7\times10^{-9}; 6.2\times10^{-9})$	$6.0\times10^{-9}(5.1\times10^{-9}; 7.0\times10^{-9})$
β	0.11(0.07; 0.20)	0.57(0.37; 0.74)
μ_{MAX}	0.12(0.08; 0.21)	0.15(0.01; 0.27)
q_0	$3.9\times10^{-8}(1.7\times10^{-8}; 6.5\times10^{-8})$	$7.8\times10^{-8}(6.4\times10^{-8}; 1.2\times10^{-7})$
Q_{init}	$4.6\times10^{-8}(1.5\times10^{-9}; 7.3\times10^{-8})$	$6.1\times10^{-9}(3.0\times10^{-9}; 2.4\times10^{-8})$
	Pyrocystis lunula	
$v_{MAX\_NO_3}$	$2.6\times10^{-6}(2.1\times10^{-6}; 3.2\times10^{-6})$	$2.7\times10^{-6}(1.1\times10^{-6}; 4.3\times10^{-6})$
β	0.18(0.17; 0.24)	0.14(0.05; 0.31)
μ_{MAX}	0.58(0.46; 0.75)	0.49(0.26; 0.72)
q_0	$4.1\times10^{-5}(2.3\times10^{-5}; 6.9\times10^{-5})$	3.6×10^{-5} $(7\times10^{-6}; 5.1\times10^{-5})$
Q_{init}	$1.8\times10^{-4}(9.5\times10^{-5}; 2.8\times10^{-4})$	$1.7\times10^{-4}(2.2\times10^{-5}; 5.5\times10^{-4})$

assuming that the variability is driven mainly by process error, we can better assess the robustness of our results than if we had simply assumed observation error only, as standard least-squares fitting does (Ives et al. 1999). For instance, two species displayed consistent sets of parameters overall, indicating good confidence in their estimated values (*Nannochloropsis oculata* and *Pyrocystis lunula*). One species, *Picochlorum atomus*, showed a large difference in estimated nitrate uptake rate ($v_{MAX\_NO_3}$), which was reconciled when the model was calibrated excluding the initially high uptake rate of nitrate for the first 2 d. This strongly suggests that the divergent estimates from the two likelihoods was due to the fact that the model lacks a mechanism to capture an initial period of very rapid nitrate uptake, a point to which we return below. Finally, one species, *Isochrysis* sp., exhibited considerable differences in the parameters for nitrite release (β) and internal nutrient status (q_0, Q_{init}); further in this section we discuss how these discrepancies were caused by the model's inability to simultaneously capture the occurrence of approximately exponential cell growth, and a transition from very low to very high nitrite release.

As noted in the Results, model selection favored estimating all nitrite-related parameters (i.e., β, $v_{MAX\_NO_2}$, and φ) only when both net medium nitrite release and uptake were sustained for > 24 h. This was not the case for *Nannochloropsis oculata*, as net nitrite release occurred only between the first and second day and was not accompanied by any significant change in medium nitrate availability or estimated internal nitrogen availability. Similarly, the functional response for nitrite uptake in *Isochrysis* sp. and *Pyrocystis lunula* did not significantly improve the total fit of the model. Therefore, these parameters were removed and a simpler model, which omits the nitrite uptake term, was used to estimate the other model parameters. When all nitrite utilization parameters could be estimated, as for *Picochlorum atomus*, they can be used to infer nitrite utilization dynamics under alternative nitrate fertilization regimes. For instance, β indicates the overall proportion of nitrate and nitrite uptake that can be released back into the medium as nitrite, when the internal quota is full. This parameter varies substantially among our study species. Though rare in the literature (Collos 1998), such information is particularly valuable. Firstly, information on phytoplankton nitrite uptake and release are required when estimating total assimilated nitrogen and primary production in areas of the ocean with high nitrite concentration (Collos 1998; Al-Qutob et al. 2002).

Secondly, an imbalance in nitrate supply can be costly for both phytoplankton aquaculture facilities and for the remediation of nitric oxide from flue gas. For aquaculture, undersupply of nitrate results in reduced biomass yields, whereas an oversupply of nitrate requires expensive wastewater treatment and can increase phytoplankton total biomass production while reducing specific lipid content (Li et al. 2008; Lardon et al. 2009). Conversely, for nitric oxide remediation of flue gas from coal-fired power stations, excessive nitrate provision can result in extracellular buildup of nitrite, driven by incomplete reduction of nitrite to ammonium and the conversion of flue-gas nitric oxide to nitrite in water (Niu and Leung 2010). Undoubtedly, some of the model's simplifying assumptions, which are adequate given the axenic cultures that we used, would need to be modified for application to natural ecosystems in situ. For instance, in natural systems, the activity of nitrifying and denitrifying bacteria significantly contribute to the dynamics of total available inorganic nitrogen (Zehr and Kudela 2011).

Our model offers an additional tool to investigate nutrient uptake and how it influences population growth and nitrite utilization. For instance, in the present model, there are two main factors determining changes in extracellular nitrite concentration for a species. The first factor is extracellular nitrate availability. Simulating population growth using observation-model parameters for *Picochlorum atomus* showed an increase in external nitrite production proportional to extracellular nitrate availability (Fig. 5). This result is consistent with a number of field and laboratory studies investigating nitrite excretion by phytoplankton species (Wada and Hattori 1971; Olson et al. 1980; Collos 1982*a*). Nitrite is released into the medium when the reduction of nitrate to nitrite proceeds faster than that of nitrite to ammonium, and the cell releases nitrite to avoid the consequences of internal over-nitrification (Collos 1982*a*). This suggests that the model's structure captures qualitative aspects of phytoplankton–nitrite dynamics that are relevant beyond the particular cultures examined here.

Although we did not make direct measurements of internal nitrogen quota, the estimated quota parameters are consistent with available evidence. For instance, our estimated values of Q_{init} and q_0 span a range comparable to that of published data on the relationship between cell volume and internal nitrogen quota (Shuter 1978). In our study, cell volume spans four orders of magnitude difference between the smallest (*Nannochloropsis oculata*; Brown 1991; Lourenco et al. 2002) and largest (*Pyrocystis lunula*; Shuter 1978) species, with a corresponding three-order-of-magnitude difference in estimated Q_{init} and q_0 values for these species. Similarly, the power-law allometric relationship estimated from phytoplankton data by Shuter (1978) has a scaling exponent of ~ 0.7, implying a change in internal nitrogen quota of just under three orders of magnitude for a four-order-of-magnitude change in cell volume. Moreover, our parameter estimates implied a decrease in internal nitrogen through time in three of our four species (Fig. 3A,B,D). Although this may seem counterintuitive (since external nitrate remained abundant throughout the experiment), internal quota is a per-cell quantity: total internal nitrogen (quota times population size) actually increases during the experiment for all species. Per-cell quota reflects an equilibrium between per-cell nitrogen uptake and its allocation to population growth; quota concentration will therefore decrease when above its equilibrium value for those conditions, even when external nitrogen is highly abundant (see Chu et al. 2007 for an empirical example). Moreover, Chu et al. (2007) observed that population growth shifts from fast to slow as internal quota decreases towards its equilibrium value: we also observed this coincident decrease in growth rate in the three species whose internal quotas were predicted to have decreased during our experiment, but not in the species whose internal quota was predicted to have increased (compare Figs. 2, 3). This further suggests that our model predicts realistic internal growth dynamics.

Model simulations can be employed to explore differences in nitrite utilization under different scenarios of internal nitrogen availability. For example, the observation-error parameter estimates for *Picochlorum atomus* predict that cultures with lower intracellular nitrogen storage should excrete significantly less nitrite overall than cultures with filled nitrogen stores (Fig. 6). Nitrite release decreased almost linearly with starvation time from 0 to 5 d in the marine diatom *Phaeodactylum tricornutum* (Collos 1982*a*). Furthermore, observations for *Skeletonema costatum* and *Prorocentrum minimum* are also consistent with the model: Cultures resupplied with nitrate after 12–24 h of starvation show higher nitrite excretion compared to cultures starved for longer periods (Serra et al. 1978; Martinez 1991; Sciandra and Amara 1994). Sometimes the reduced nitrite release in starved cultures was concurrent with a reduction in nitrate uptake for the first 1–2 d, perhaps caused by an acclimatization period necessary for the culture to adapt to the new nutrient regime (Collos 1982*a*; Martinez 1991; Sciandra and Amara 1994). While the present model incorporates a mechanism that reduces nitrite release in response to a decrease in nitrate uptake (Eq. 1f), it also suggests an additional explanation for the predicted lower nitrite release by nutrient-starved cultures (Fig. 6). Specifically, using the observation model parameters for *Picochlorum atomus*, model dynamics under nitrogen-replete intracellular storage conditions (solid line in Fig. 6A) indicate that initially most of the excess internal quota energy is used for rapid growth (solid line in Fig. 6D). The same species simulated under nitrogen-starved conditions shows that initially most of the nitrate taken up may be used to replenish depleted stores (dashed line in Fig. 6A), rather than being utilized for population growth (dashed line in Fig. 6D). This results in monotonically decreasing medium nitrite (Fig. 6B), no net per-capita nitrite excretion (Fig. 6C), and lower biomass production rate (Fig. 6D). The initial increase in internal quota detected for the simulated nutrient-starved culture (Fig. 6A) is known as acclimation period or lag phase, and is often detected in phytoplankton dynamics when relocated to new environmental conditions (Fogg and Thake 1987). Consistent with the model, laboratory studies have shown that nitrogen limitation leads to no or reduced culture growth, and the flow of fixed carbon

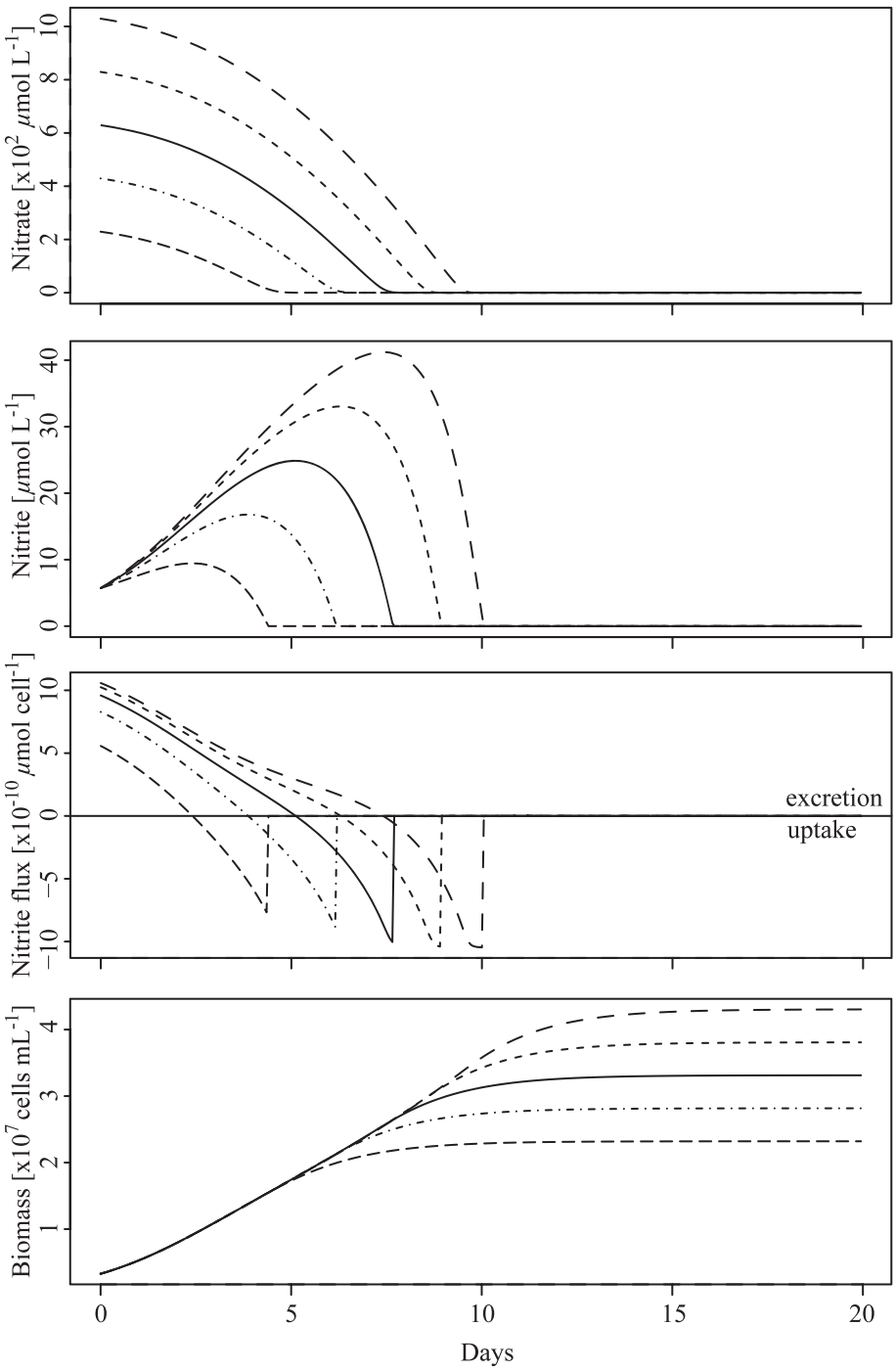

Fig. 5. Simulated effects of different initial nitrate levels on the dynamics of (A) external nitrate, (B) external nitrite, (C) per capita nitrite excretion (positive) and uptake (negative), and (D) biomass concentration. Demographic parameters and initial values for biomass, nitrogen quota, and extracellular nitrite concentration are based on the observation-error estimates for *Picochlorum atomus* (*see* Table 5). The baseline (middle) trajectory corresponds to the estimated initial nitrate levels from the *Picochlorum atomus* experiment (Table 5). Trajectories were generated with Eq. 1, using package deSolve in R (Soetaert et al. 2010).

from photosynthesis is diverted and stored in the form of lipids or carbohydrates (Rodolfi et al. 2009; Mata et al. 2010). For this reason, many aquaculture systems include nitrogen-limiting conditions as part of the phytoplankton cultivation cycle in order to optimize accumulation of desired end products such as storage lipids (e.g., triacylglycerols in Thomas et al. 1984) or carbohydrates (e.g., starch, paramylon, or chrysolaminarin in Adam 1997).

Although the model captures the broad-scale dynamics of the system, there are two ways in which the data deviate

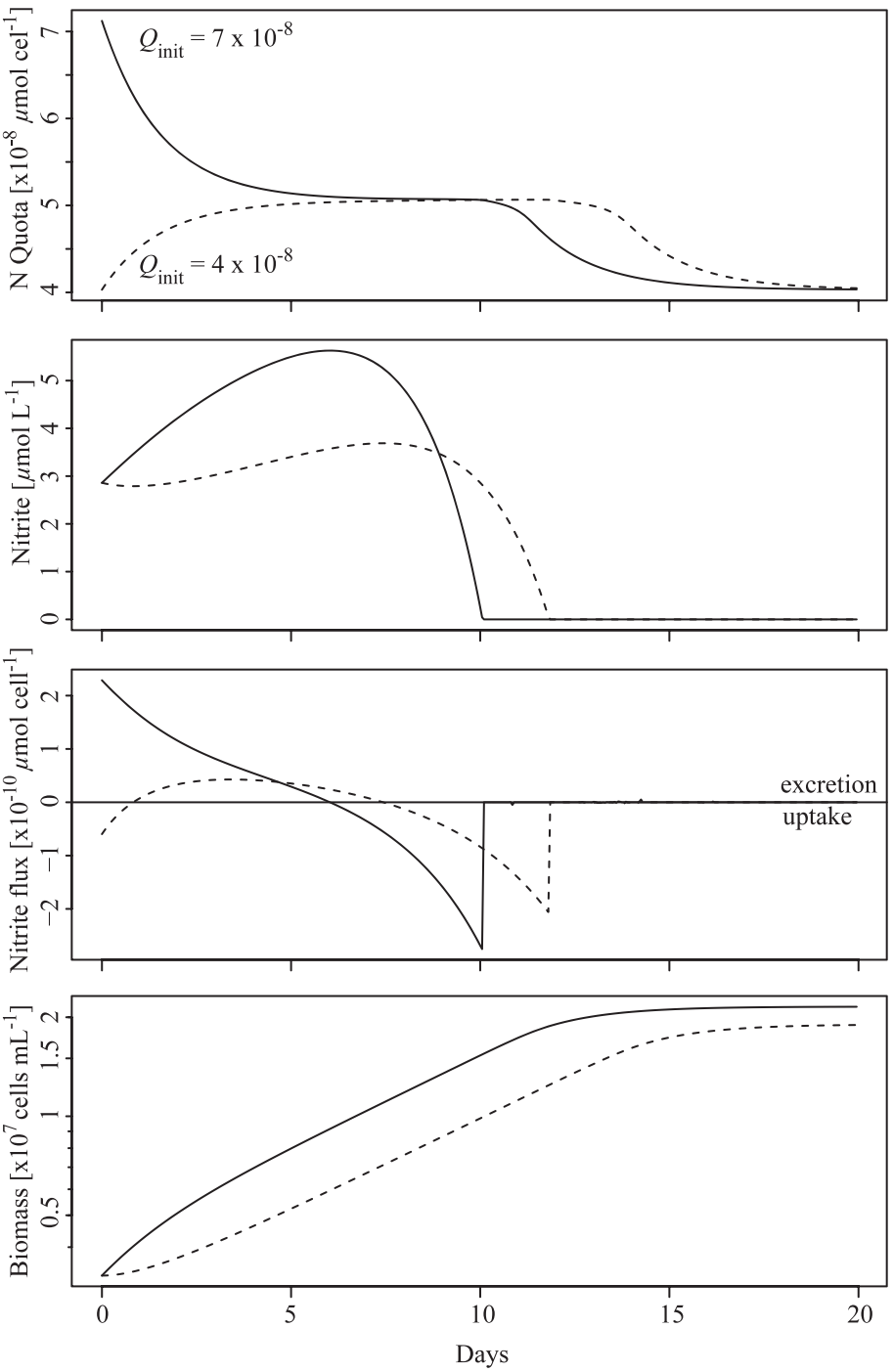

Fig. 6. Simulated effects for two different scenarios of initial per capita nitrogen quota on the dynamics of (A) internal nitrogen, (B) external nitrite, (C) per-capita nitrite excretion (positive) and uptake (negative), and (D) biomass concentration (log-transformed). Demographic parameters and initial values for biomass, extracellular nitrate and nitrite concentrations are based on the estimates for *Picochlorum atomus* using the observation-error model (Table 5). (A) Labels indicate initial values of internal quota (Q_{init}). Trajectories were generated with Eq. 1, using package deSolve in R (Soetaert et al. 2010).

systematically from the model. These deviations provide clues as to how the framework presented here might be refined in future work. The first is that, for both *Picochlorum atomus* and *Nannochloropsis oculata*, the data show an elevated rate of medium nitrate depletion over the first 2–3 d (Fig. 4A,B), which the model does not capture. To cope with patchy nutrient distributions in nature, two nutrient uptake systems with different uptake kinetics have evolved (Crawford et al. 2000). Low nutrient availability ($\sim$ 100 μmol L^{-1}) induces the expression of high-affinity

uptake systems, which are saturable and characterized by a maximum uptake rate limiting assimilation (Crawford et al. 2000; Smith et al. 2009). High nutrient availability ($\sim$ 1000 μmol L^{-1}) induces the expression of low-affinity uptake systems, which are non-saturable and cells take up nutrients in proportion to the nutrient concentration in the environment (Crawford et al. 2000; Collos et al. 2005). The observed rapid uptake of nitrate by *Picochlorum atomus* and *Nannochloropsis oculata* from days 1 to 3 may indicate uptake via low-affinity systems, while slower nitrate uptake from day 3 onward may reflect the shift to a high-affinity uptake system (Fig. 4A,B). Similar multiphase nutrient utilization patterns have been recorded for several phytoplankton species (*see* Collos et al. 2005 for review). Thus, one area for refinement of our approach would be to explicitly model switching between low-affinity and high-affinity uptake systems.

The second area of systematic deviation between the data and the model is in the medium nitrite dynamics for *Isochrysis* sp. Specifically, nitrite secretion was low at the beginning of the experiment, then increased rapidly toward the end (Fig. 1C). These dynamics are unusual for phytoplankton species. Typically, the period of highest nitrite release coincides with the period of greatest nitrate availability (Collos 1998), which, in our cultures, occurred at the beginning of the experiment (Fig. 4C). Growth patterns (Fig. 2C), internal quota (Fig. 3C), and nitrate utilization (Fig. 4C) for *Isochrysis* sp. cultures suggest that the mother cultures used for inoculation were nitrate-replete. Therefore, according to Collos (1998), and as observed for *Picochlorum atomus*, a higher nitrite secretion was expected at the start of the experiment, which should have been utilized as a nitrogen source later when extracellular nitrate became limiting. Partial light limitation of photosynthesis (through self-shading due to population growth, and therefore reduced provision of reduced ferredoxin) could produce, in principle, a sudden, rapid increase in the rate of nitrite release, as we observed from day 13 onward for *Isochrysis* sp. (Fig. 1C; Agusti 1991). However, light limitation typically results in reduced population growth rates (Harrison et al. 1990), which was not observed for *Isochrysis* sp. during the period of rapid nitrite release. For the other species, we did not observe any anomalous increases in nitrite release associated with a slowing of population growth, as we might expect under light limitation. We therefore conclude that light limitation is unlikely to have substantially affected our culture dynamics. Nevertheless, because light limitation is common in nature, and also can occur in industrial and laboratory settings, an extension of the model to incorporate effects of light limitation on the dynamics of nitrite release is an important area for further work.

Our extension of the Legovic and Cruzado (1997) model to characterize nitrite utilization captured the main features of population, nitrate, and nitrite dynamics for four phytoplankton species exhibiting very different patterns of population growth, and nutrient assimilation and release, despite using few parameters, relative to other models that account for nitrite dynamics. Our approach allowed estimation of most model parameters, except when particular phases of nutrient utilization did not occur (e.g., depletion of nitrite in *Isochrysis* sp. and *Pyrocystis lunula*). For *Picochlorum atomus*, which exhibited both net nitrite excretion and uptake from the culture medium, we were able to use our fitted model to simulate coupling between population growth and nutrient assimilation under alternative conditions, and thereby reproduce important qualitative features of population and nutrient dynamics in field and laboratory studies. The capacity of the model to fit empirical data for species exhibiting such a broad range of nitrite dynamics suggests that our approach could be a useful foundation for further development and testing.

Acknowledgments

We are grateful to the North Queensland Algal Identification Facility. In particular, we thank Jessica Maddams, Stan Hudson, and Saskia De Jong for their support in laboratory procedures. We also thank the Ecological Modeling Research Group at James Cook University, especially Loic Thibaut, for helpful advice and constructive criticism. Igor Pirozzi, Jeremy VanDerWal, and Andrew Krockenberger provided helpful comments on an earlier draft of the work. We also thank two anonymous reviewers for constructive comments on the manuscript. This research contributes to the MBD Energy Research and Development program for Microalgal Carbon Capture and Storage supported by the Advanced Manufacturing Cooperative Research Centre, funded through the Australian Government's Cooperative Research Centre Scheme. The Australian Research Council (ARC) and James Cook University provided additional research support.

References

Adam, M. S. 1997. Metabolic response of the halotolerant green alga *Dunaliella bardawil* to nitrogen : phosphorus ratios in batch culture. Folia Microbiol. **42:** 357–360, doi:10.1007/BF02816950

Agusti, S. 1991. Light environment within dense algal populations: Cell-size influences on self-shading. J. Plankton Res. **13:** 863–871, doi:10.1093/plankt/13.4.863

Al-Qutob, M., C. Häse, M. M. Tilzer, and B. Lazar. 2002. Phytoplankton drives nitrite dynamics in the Gulf of Aqaba, Red Sea. Mar. Ecol. Prog. Ser. **239:** 233–239, doi:10.3354/meps239233

Bolker, B. 2008. Dynamic models, p. 445–470. *In* B. Bolker [ed.], Ecological models and data in R. Princeton Univ. Press.

Bozdogan, H. 1987. Model selection and Akaike Information Criterion (AIC): The general-theory and its analytical extensions. Psychometrika **52:** 345–370, doi:10.1007/BF02294361

Brown, M. R. 1991. The amino-acid and sugar composition of 16 species of microalgae used in mariculture. J. Exp. Mar. Biol. Ecol. **145:** 79–99, doi:10.1016/0022-0981(91)90007-J

Campbell, W. H. 1999. Nitrate reductase structure, function and regulation: Bridging the gap between biochemistry and physiology. Annu. Rev. Plant. Physiol. Plant Mol. Biol. **50:** 277–303, doi:10.1146/annurev.arplant.50.1.277

Carvalho, A. P., L. A. Meireles, and F. X. Malcata. 1998. Rapid spectrophotometric determination of nitrates and nitrites in marine aqueous culture media. Analusis **26:** 347–351, doi:10.1051/analusis:1998183

Chu, Z. S., X. C. Jin, B. Yang, and Q. R. Zeng. 2007. Buoyancy regulation of *Microcystis flos-aquae* during phosphorus-limited and nitrogen-limited growth. J. Plankton Res. **29:** 739–745, doi:10.1093/plankt/fbm054

Collos, Y. 1982*a*. Transient situations in nitrate assimilation by marine diatoms. 2. Changes in nitrate and nitrite following a nitrate perturbation. Limnol. Oceanogr. **27:** 528–535, doi:10.4319/lo.1982.27.3.0528

———. 1982*b*. Transient situations in nitrate assimilation by marine diatoms. 3. Short-term uncoupling of nitrate uptake and reduction. J. Exp. Mar. Biol. Ecol. **62:** 285–295, doi:10.1016/0022-0981(82)90208-8

———. 1998. Nitrate uptake, nitrite release and uptake, and new production estimates. Mar. Ecol. Prog. Ser. **171:** 293–301, doi:10.3354/meps171293

———, A. Vaquer, and P. Souchu. 2005. Acclimation of nitrate uptake by phytoplankton to high substrate levels. J. Phycol. **41:** 466–478, doi:10.1111/j.1529-8817.2005.00067.x

Crawford, N. M., M. L. Kahn, T. Leustek, and S. R. Long. 2000. Nitrogen and sulfur, p. 786–849. *In* B. B. Buchanan, W. Gruissem, and R. L. Jones [eds.], Biochemistry and molecular biology of plants. American Society of Plant Physiologists.

Cresswell, R. C., and P. J. Syrett. 1982. The uptake of nitrite by the diatom *Phaeodactylum*: Interactions between nitrite and nitrate. J. Exp. Bot. **33:** 1111–1121, doi:10.1093/jxb/33.6.1111

Cusson, M., and E. Bourget. 2005. Global patterns of macroinvertebrate production in marine benthic habitats. Mar. Ecol. Prog. Ser. **297:** 1–14, doi:10.3354/meps297001

Dennis, B., J. M. Ponciano, and M. L. Taper. 2010. Replicated sampling increases efficiency in monitoring biological populations. Ecology **91:** 610–620, doi:10.1890/08-1095.1

Dortch, Q. 1990. The interaction between ammonium and nitrate uptake in phytoplankton. Mar. Ecol. Prog. Ser. **61:** 183–201, doi:10.3354/meps061183

———, P. A. Thompson, and P. J. Harrison. 1991. Variability in nitrate uptake kinetics in *Thalassiosira pseudonana* (Bacillariophyceae). J. Phycol. **27:** 35–39, doi:10.1111/j.0022-3646.1991.00035.x

Droop, M. R. 1973. Some thoughts on nutrient limitation in algae. J. Phycol. **9:** 264–272.

Dugdale, R. C. 1967. Nutrient limitation in the sea: Dynamics, identification, and significance. Limnol. Oceanogr. **12:** 685–695, doi:10.4319/lo.1967.12.4.0685

Fierro, S., M. D. P. Sánchez-Saavedra, and C. Copalcua. 2008. Nitrate and phosphate removal by chitosan immobilized *Scenedesmus*. Bioresource Technol. **99:** 1274–1279, doi:10.1016/j.biortech.2007.02.043

Flynn, K. J., and K. Flynn. 1998. Release of nitrite by marine dinoflagellates: Development of a mathematical simulation. Mar. Biol. **130:** 455–470, doi:10.1007/s002270050266

Fogg, G. E., and B. Thake. 1987. Cultures of limited volume, p. 12–43. *In* G. E. Fogg and B. Thake [eds.], Algal cultures and phytoplankton ecology. Univ. of Wisconsin Press.

Galván, A., and E. Fernández. 2001. Eukaryotic nitrate and nitrite transporters. Cell. Mol. Life Sci. **58:** 225–233, doi:10.1007/PL00000850

Guerrero, M. G., J. M. Vega, and M. Losada. 1981. The assimilatory nitrate-reducing system and its regulation. Annu. Rev. Plant Physiol. Plant Mol. Biol. **32:** 169–204.

Harrison, P. J., and J. A. Berges. 2005. Marine culturing media, p. 21–34. *In* R. A. Andersen [ed.], Algal culturing techniques. Elsevier/Academic Press.

———, P. A. Thompson, and G. S. Calderwood. 1990. Effects of nutrient and light limitation on the biochemical composition of phytoplankton. J. Appl. Phycol. **2:** 45–56, doi:10.1007/BF02179768

Hilborn, R., and M. Mangel. 1997. The confrontation: Likelihood and maximum likelihood, p. 131–171. *In* R. Hilborn and M. Mangel [eds.], The ecological detective: Confronting models with data. Princeton Univ. Press.

Ives, A. R., S. R. Carpenter, and B. Dennis. 1999. Community interaction webs and zooplankton responses to planktivory manipulations. Ecology **80:** 1405–1421, doi:10.1890/0012-9658(1997)080[1405:CIWAZR]2.0.CO;2

Klausmeier, C. A., E. Litchman, and S. A. Levin. 2004. Phytoplankton growth and stoichiometry under multiple nutrient limitation. Limnol. Oceanogr. **49:** 1463–1470, doi:10.4319/lo.2004.49.4_part_2.1463

Kutner, M., C. Nachtsheim, J. Neter, and W. Li. 2004. Applied linear statistical models, 5th ed. McGraw-Hill/Irwin.

Lardon, L., A. Hélias, B. Sialve, J. P. Stayer, and O. Bernard. 2009. Life-cycle assessment of biodiesel production from microalgae. Environ. Sci. Technol. **43:** 6475–6481, doi:10.1021/es900705j

Legovic, T., and A. Cruzado. 1997. A model of phytoplankton growth on multiple nutrients based on the Michaelis-Menten-Monod uptake, Droop's growth and Liebig's law. Ecol. Model. **99:** 19–31, doi:10.1016/S0304-3800(96)01919-9

Lehman, J. T., D. B. Botkin, and G. E. Likens. 1975. The assumptions and rationales of a computer model of phytoplankton population dynamics. Limnol. Oceanogr. **20:** 343–364, doi:10.4319/lo.1975.20.3.0343

Li, Y. Q., M. Horsman, B. Wang, N. Wu, and C. Q. Lan. 2008. Effects of nitrogen sources on cell growth and lipid accumulation of green alga *Neochloris oleoabundans*. Appl. Microbiol. Biotechnol. **81:** 629–636, doi:10.1007/s00253-008-1681-1

Lourenco, S. O., E. Barbarino, J. Mancini-Filho, K. P. Schinke, and E. Aidar. 2002. Effects of different nitrogen sources on the growth and biochemical profile of 10 marine microalgae in batch culture: An evaluation for aquaculture. Phycologia **41:** 158–168, doi:10.2216/i0031-8884-41-2-158.1

Mackey, K. R. M., L. Bristow, D. R. Parks, M. A. Altabet, A. F. Post, and A. Paytan. 2011. The influence of light on nitrogen cycling and the primary nitrite maximum in a seasonally stratified sea. Prog. Oceanogr. **91:** 545–560, doi:10.1016/j.pocean.2011.09.001

Martinez, R. 1991. Transient nitrate uptake and assimilation in *Skeletonema costatum* cultures subject to nitrate starvation under low irradiance. J. Plankton Res. **13:** 499–512, doi:10.1093/plankt/13.3.499

Mata, T. M., A. A. Martins, and N. S. Caetano. 2010. Microalgae for biodiesel production and other applications: A review. Renew. Sust. Energ. Rev. **14:** 217–232, doi:10.1016/j.rser.2009.07.020

Niu, H. J. Y., and D. Y. C. Leung. 2010. A review on the removal of nitrogen oxides from polluted flow by bioreactors. Environ. Rev. **18:** 175–189, doi:10.1139/A10-007

Olson, R. J., J. B. Soohoo, and D. A. Kiefer. 1980. Steady-state growth of the marine diatom *Thalassiosira pseudonana*: Uncoupled kinetics of nitrate uptake and nitrite production. Plant Physiol. **66:** 383–389, doi:10.1104/pp.66.3.383

Petersen, K. B., and M. S. Pedersen. 2008. The matrix cookbook [Internet]. Technical report. Copenhagen, Denmark: Technical Univ. of Denmark [accessed 2011 September 26]. 67 p. Available from http://orion.uwaterloo.ca/~hwolkowi/matrixcookbook.pdf

Platt, T., W. G. Harrison, M. R. Lewis, W. K. W. Li, S. Sathyendranath, R. E. Smith, and A. F. Vezina. 1989. Biological production of the oceans: The case for a consensus. Mar. Ecol. Prog. Ser. **52:** 77–88, doi:10.3354/meps052077

R Development Core Team. 2011. R: A language and environment for statistical computing [Internet]. Vienna, Austria: R Foundation for Statistical Computing [accessed 2012 February 11], Available from http://www.R-project.org

Rodolfi, L., G. C. Zittelli, N. Bassi, G. Padovani, N. Biondi, G. Bonini, and M. R. Tredici. 2009. Microalgae for oil: Strain selection, induction of lipid synthesis and outdoor mass cultivation in a low-cost photobioreactor. Biotechnol. Bioeng. **102:** 100–112, doi:10.1002/bit.22033

Sciandra, A., and R. Amara. 1994. Effects of nitrogen limitation on growth and nitrite excretion rates of the dinoflagellate *Prorocentrum minimum*. Mar. Ecol. Prog. Ser. **105:** 301–309, doi:10.3354/meps105301

Serra, J. L., M. J. Llama, and E. Cadenas. 1978. Nitrate utilization by diatom *Skeletonema costatum*. 1. Kinetics of nitrate uptake. Plant Physiol. **62:** 987–990, doi:10.1104/pp.62.6.987

Shuter, B. J. 1978. Size dependence of phosphorus and nitrogen subsistence quotas in unicellular microorganisms. Limnol. Oceanogr. **23:** 1248–1255, doi:10.4319/lo.1978.23.6.1248

Smith, S. L., and Y. Yamanaka. 2007. Optimization-based model of multinutrient uptake kinetics. Limnol. Oceanogr. **52:** 1545–1558, doi:10.4319/lo.2007.52.4.1545

———, ———, M. Pahlow, and A. Oschlies. 2009. Optimal uptake kinetics: Physiological acclimation explains the pattern of nitrate uptake by phytoplankton in the ocean. Mar. Ecol. Prog. Ser. **384:** 1–12, doi:10.3354/meps08022

Soetaert, K., R. T. Petzoldt, and W. Setzer. 2010. Solving differential equations in R: Package deSolve. J. Stat. Softw. **33:** 1–25. http://www.jstatsoft.org/v33/i09/

Thomas, W., T. Tornabene, and J. Weissman. 1984. Screening for lipid yielding microalgae: Activities for 1983. Final report SERI/STR-231-2207. Solar Energy Research Institute, Colorado, U.S.A.

Throndsen, J. 1978. Preservation and storage, p. 69–74. *In* A. A. Sournia [ed.], Phytoplankton manual: Monographs on oceanographic methodology. UNESCO.

Turchin, P. 1996. Nonlinear time-series modeling of vole population fluctuations. Res. Popul. Ecol. **38:** 121–132, doi:10.1007/BF02515720

———. 2003. Single species populations, p. 47–76. *In* P. Turchin [ed.], Complex population dynamics: A theoretical/empirical synthesis. Princeton Univ. Press.

Wada, E., and A. Hattori. 1971. Nitrite metabolism in the euphotic layer of the central North Pacific Ocean. Limnol. Oceanogr. **16:** 766–772, doi:10.4319/lo.1971.16.5.0766

Yang, J., M. Xu, X. Z. Zhang, Q. A. Hu, M. Sommerfeld, and Y. S. Chen. 2011. Life-cycle analysis on biodiesel production from microalgae: Water footprint and nutrients balance. Bioresource Technol. **102:** 159–165, doi:10.1016/j.biortech.2010.07.017

Zehr, J. P., and R. M. Kudela. 2011. Nitrogen cycle of the open ocean: From genes to ecosystems. Annu. Rev. Mar. Sci. **3:** 197–225, doi:10.1146/annurev-marine-120709-142819

Zheng, J., J. M. Hao, B. Wang, and C. Shui. 2011. Bioremediation of aquiculture wastewater by microalgae *Isochrysis zhanjiangensis* and production of the biomass material, p. 491–495. *In* Y. M. Wu [ed.], Components, packaging and manufacturing technology. Key engineering materials. Trans Tech Publications.

Associate editor: Robert R. Bidigare

Received: 07 March 2012
Accepted: 07 June 2012
Amended: 21 June 2012